Slip-induced dynamics of patterned and Janus-like spheres in laminar flows

Geoff R. Willmott*
Industrial Research Limited, 69 Gracefield Road, Lower Hutt 5040, New Zealand
(Received 6 March 2009; published 17 June 2009)

Calculations of force and torque on a sphere with inhomogeneous slip boundary conditions are presented. A theoretical approach introduced previously is employed to explicitly explore two types of azimuthally symmetric boundary-condition patterning of high practical importance. The first is a discontinuous binary surface while the second involves continuously varying slip patterned in stripes, with arbitrary periodicity. These geometries mimic anisotropic spheres, as well as superhydrophobic surfaces applied to a sphere. The dynamics apply for unbounded uniform flow and pure rotational flow of a Newtonian fluid at low Reynolds number. In unbounded uniform flow, torque is maximized for an ideal Janus sphere with a discontinuous equatorial transition between regions of slip and no slip.

DOI: 10.1103/PhysRevE.79.066309 PACS number(s): 47.85.−g, 83.50.Lh, 83.10.Pp

I. INTRODUCTION

When the nonslip boundary condition (NSBC) applies at the surface of a solid sphere in unbounded uniform Newtonian flow, the sphere experiences zero torque along with a drag force given by the well-known Stokes formula. The dynamics of such a sphere change when there is uniform nonzero slip over the surface, creating a "lubrication" force, or reduction in the drag force [1]. Slip occurs when the fluid immediately adjacent to a solid surface has nonzero tangential motion relative to that surface, usually characterized by slip "length" b [2]. In addition to uniform spheres, full first-order dynamics have been calculated for uniform slip on a nearly spherical particle [3] and nearly uniform slip on a spherical particle [4]. In the latter case, it was predicted that a sphere with asymmetric slip boundary conditions can experience a torque in uniform flow. This result has important implications for two fields of high current interest in nanofluidics and microfluidics: fundamental studies of nonzero surface slip and research into asymmetric spherical particles, typified by "Janus" spheres.

Modern reviews [2,5] have summarized experimental violations of the NSBC ($b=0$), which was assumed to apply universally to Newtonian fluids at an impermeable solid surface for most of the 20th century. It has recently become clear that Newtonian slip occurs in two distinct regimes, separated by length scale. "Intrinsic" slip yields slip lengths of the order of 10 nm at molecularly smooth hydrophobic surfaces [6,7]. "Effective" slip, which can generate slip lengths of the order of microns or larger, concerns measurements of fluid flow some distance from a surface, independent of the phenomenology close to the surface itself. Effective slip is most commonly used to describe ultrahydrophobic or superhydrophobic surfaces. These surfaces occur naturally or are engineered in various forms [8–11], and are typically characterized by regular or irregular patterns of surface roughness, along with hydrophobicity. Some regular patterns have been explored theoretically, including flow over planar surfaces consisting of a regular pattern of stripes or ribs [8,12–15], and flow through a cylinder with similar internal surfaces [16].

Fabrication of small anisotropic particles is a very topical area that has been placed into a conceptual framework by Glotzer and Solomon [17]. Small particles of spherical geometry are reasonably easy to fabricate due to minimization of surface energy, and are ubiquitous in many branches of fluidics research and applications. Janus spheres are a special type of anisotropic sphere for which the properties of one hemisphere differ from those of the other. The range of preparation pathways and physical characteristics of Janus particles is strikingly diverse [18–34], covering particle sizes from 2 nm functionalized nanoparticles [20] to 200 μm colloidal dispersions [21]. Several types of Janus particle are amphiphilic, consisting of surface areas that are hydrophobic (therefore potentially exhibiting intrinsic slip) and hydrophilic [18,23,25,26,30,35]. Areal surface coverage for a binary particle can be far from equally divided, and has been actively controlled in some cases [26,30,33]. Well-defined families of particles with ternary [33] or periodic [17,29] surface patterning have also been produced. Application areas for Janus particles match the diversity of the particles themselves [18,19] but often relate to their role at colloidal boundaries [25], as self-assembling components in complex superstructures [17,27], or in various optofluidic roles [21,22]. Janus particles can be manipulated using externally applied fields [24,35] but the dynamics introduced in [4] simply apply to any Janus particle in a Newtonian fluid.

The present work explores the dynamics of spheres using the general theoretical approach that was introduced in [4], and is recounted in Sec. II. The remainder of the paper extends that general approach to specific asymmetric surface patterns characterized by variable slip length. Force and torque are presented for spheres in unbounded uniform flow as well as purely rotational flow using two types of boundary condition. The first consists of two homogeneous surface areas separated by a slip length discontinuity. The second explores continuously varying slip with pattern periodicity. Boundary-condition patterns are azimuthally symmetric and mimic the patterning of practical Janus-like spheres, as well as superhydrophobic surfaces applied to a sphere. In the course of this work, two of the anisotropy "dimensions" identified in Glotzer and Solomon's framework [17] are ad-

*FAX: (64) (0)4 931 3117; g.willmott@irl.cri.nz

dressed: surface coverage (patchiness) and pattern quantization, as applied to the surface of spheres.

II. BACKGROUND

The analysis detailed in [4] concerns an impermeable sphere in an incompressible Newtonian fluid at low Reynolds number. The slip boundary condition is defined in the conventional manner for the rest frame of the wall [2,36,37],

$$v_{\parallel} = b\mathbf{n} \cdot [\nabla \mathbf{v} + (\nabla \mathbf{v})^T] \cdot (\mathbf{I} - \mathbf{nn}), \tag{1}$$

where $v_{\parallel}$ is the component of the fluid velocity field $\mathbf{v}$ which is tangent to a solid surface, $\mathbf{n}$ is the unit normal to the surface, and the parameter b is the slip length. For an inhomogeneous boundary condition on a spherical surface, b can be replaced by the quantity $bf(\theta,\phi)$, where θ and ϕ are spherical polar coordinates. The magnitude of $f(\theta,\phi)$ is of $O(1)$, and it can be expanded in terms of surface spherical harmonics, such that $f(\theta,\phi)=\Sigma_{k=0}^{\infty} f_k(\theta,\phi)$. When b is small compared with sphere radius a, then $b \approx b_{\parallel}$, where $b_{\parallel}$ is the slip length corrected for surface curvature [37]. In this limit, the perturbed flow field around the sphere, and the force and torque on the sphere, can be expanded in powers of $\epsilon = -(b_{\parallel}/a)$, where $|\epsilon| \ll 1$. For example, the force on a sphere can be written as

$$\mathbf{F} = \mathbf{F}^{(0)} + \epsilon \mathbf{F}^{(1)} + O(\epsilon^2). \tag{2}$$

Following [3], the full resistance tensors in a fluid of viscosity η, where the sphere is subjected to an unbounded uniform flow $\mathbf{U}$ and a rotational flow $\boldsymbol{\omega}$, are

$$\begin{pmatrix} \mathbf{F}^{(i)} \\ \mathbf{T}^{(i)} \end{pmatrix} = \begin{pmatrix} 6\pi\eta a \boldsymbol{\Phi}^{(i)} & 6\pi\eta a^2 \mathbf{D}^{(i)} \\ 6\pi\eta a^2 \mathbf{C}^{(i)} & 8\pi\eta a^3 \boldsymbol{\Omega}^{(i)} \end{pmatrix} \cdot \begin{pmatrix} \mathbf{U} \\ \boldsymbol{\omega} \end{pmatrix}. \tag{3}$$

$\mathbf{F}^{(0)}$ is equal to the well-known Reynolds drag formula for unbounded uniform flow. The general first-order solutions are [4]

$$\Phi_{ij}^{(1)} = \delta_{ij} f_0 - \frac{1}{10} \nabla_i \nabla_j (r^2 f_2), \tag{4}$$

$$C_{ij}^{(1)} = D_{ij}^{(1)} = -\varepsilon_{ijk} \nabla_k (r f_1), \tag{5}$$

and

$$\Omega_{ij}^{(1)} = -3\left(\delta_{ij} f_0 - \frac{1}{10} \nabla_i \nabla_j (r^2 f_2) \right), \tag{6}$$

where δ_{ij} is the Kronecker delta, ε_{ijk} is the Levi-Civita permutation symbol, and tensor components are given in a Cartesian frame.

III. BINARY DISCONTINUOUS TRANSITION

The first type of boundary-condition pattern explicitly considered concerns an abrupt (discontinuous) junction between homogeneous surface areas (Fig. 1),

$$f(\theta,\phi) = \begin{cases} \gamma & (0 < \theta < \theta'), \\ 1 & (\theta' < \theta < \pi). \end{cases} \tag{7}$$

This boundary condition mimics several types of sphere realized in practice, and is particularly instructive in cases

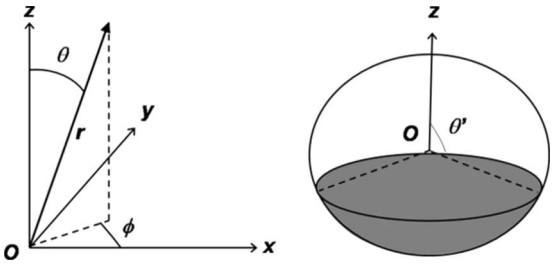

FIG. 1. (a) Cartesian (x,y,z) and spherical polar (r,θ,z) coordinate axes. The origin is at the center of a solid sphere of radius a. (b) The asymmetric geometry of the slip boundary condition from Eq. (7). Reproduced from [4].

where binary surface coverage can be measured and controlled [26,30,33]. Specifically, the value of θ' is related to the parameter α from [38] by $\theta' = 180 - \alpha$; this is not the same as the contact angle at oil-water interface [26,38]. Working in notation from [33], θ' is expressed using $R^2 \sin^2 \theta' = h_{M1} h_{M2}$. For an ideal Janus particle, in which there is a discontinuous transition between the NSBC ($\gamma = 0$) and slip length $b_{\parallel}$ at the equator ($\theta' = 90$), the specific force and torque in unbounded uniform flow were calculated in [4], and are denoted below by $\mathbf{F}_{Janus}$ and $\mathbf{T}_{Janus}$, respectively. The previous approach is now extended to include variations in γ and θ', by expanding Eq. (7) in normalized Legendre polynomials, so that

$$g_k(\theta) = \alpha_k Y_k(\theta), \tag{8}$$

where

$$Y_k(\theta) = \left(\frac{2k+1}{4\pi} \right)^{1/2} P_k(\cos\,\theta), \tag{9}$$

$$\alpha_k = \int_{-1}^{1} Y_k(\theta) g(\theta) d(\cos\,\theta), \tag{10}$$

and P_k is the Legendre polynomial of order k. Equations (3)–(6) directly relate forces and torques in unbounded uniform flow and rotational flow to the spherical harmonic terms. In unbounded uniform flow parallel to the x axis, considering terms up to first-order only,

$$\epsilon \mathbf{F}^{(1)} = \frac{b_{\parallel}}{2a} 6\pi\eta a U_x [1 + \cos\,\theta' + \gamma(1 - \cos\,\theta')] \hat{\mathbf{x}}, \tag{11}$$

and

$$\epsilon \mathbf{T}^{(1)} = -\frac{b_{\parallel}}{a} \frac{9\pi\eta a^2 U_x}{2} (1 - \cos^2\,\theta')(1 - \gamma) \hat{\mathbf{y}}. \tag{12}$$

Equations (11) and (12) are plotted in Figs. 2 and 3, respectively, with forces and torques normalized relative to the ideal Janus particle. The lubrication force is double the Janus result when the particle is uniformly slip coated ($\gamma = 1$ or $\theta' = 0°$). Lubrication falls to zero (the NSBC result) when $\gamma = 1$ and $\theta' = 180°$. For $\gamma < 1$, the magnitude of the force depends on the areal coverage and the size of the slip length parameters ($b_{\parallel}$ and γ) rather than anisotropy. In contrast, the torque applied to the sphere depends on the degree of aniso-

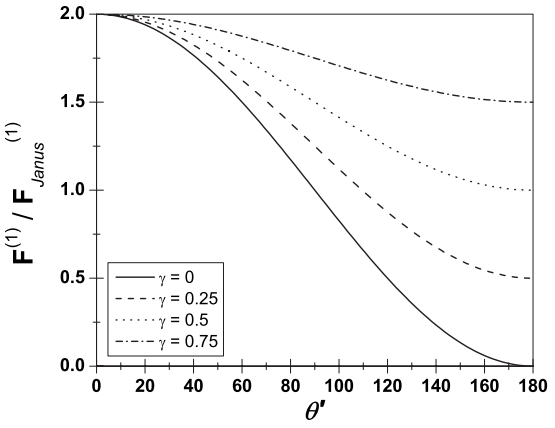

FIG. 2. The first-order force on a Janus sphere in unbounded uniform flow [Eq. (11)], plotted as a function of angular coverage (deg), with a discontinuous boundary condition given by Eq. (7). The force is normalized relative to the result for an ideal Janus sphere ($\gamma=0$, $\theta'=90$). This plot also applies to torques in purely rotational flow, in which case the vertical axis is $\mathbf{T}^{(1)}/\mathbf{T}^{(1)}_{Janus}$.

tropy, being maximized when the surface is divided in half ($\theta'=90°$) and the difference in slip lengths between the two areas is maximized ($\gamma=0$). As expected, there is zero torque when the sphere is uniformly coated ($\gamma=1$ or $\theta'=0°, 180°$). In the case of purely rotational flow $\boldsymbol{\omega}$, Figs. 2 and 3 apply, respectively, to torques and forces, where the vertical axis is given by the first-order term divided by the ideal Janus result. Therefore the degree of anisotropy determines the force in rotational flow, whereas the torque depends on total areal coverage of slip.

IV. CONTINUOUS PERIODIC PATTERN

The second specific set of boundary conditions (Fig. 4), also invariant in the azimuthal (ϕ) coordinate, describes continuous periodic variation in slip length over the spherical

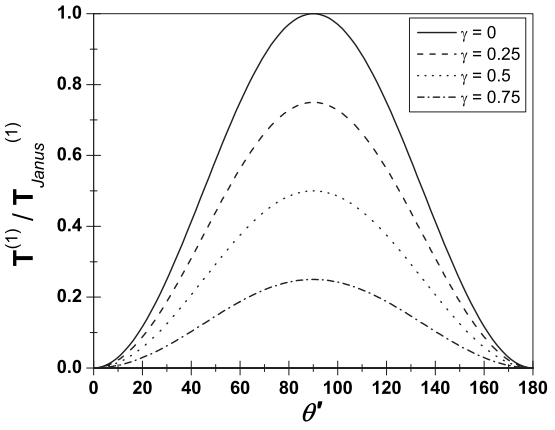

FIG. 3. The first-order torque on a Janus sphere in unbounded uniform flow [Eq. (12)], plotted as a function of angular coverage, with a discontinuous boundary condition given by Eq. (7). The torque is normalized relative to an ideal Janus sphere ($\gamma=0$, $\theta'=90$). This plot also applies to forces in purely rotational flow, in which case the vertical axis is $\mathbf{F}^{(1)}/\mathbf{F}^{(1)}_{Janus}$.

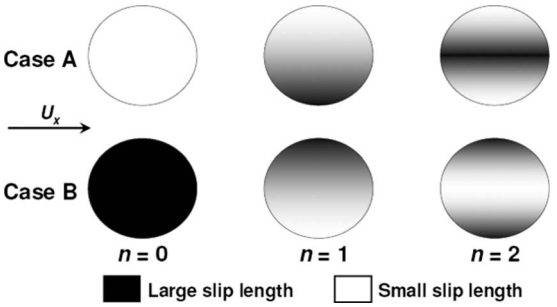

FIG. 4. Examples of continuous periodic surface slip geometries. Cases A and B refer to Eqs. (13) and (14), respectively, and shading is indicative of relative slip length. The direction of unbounded uniform flow along the Cartesian x axis (U_x) is indicated.

surface. For cases A and B, respectively, the function $f(\theta,\phi)$ as defined above is replaced with

$$g = \sin^2\left(\frac{n\theta}{2}\right), \tag{13}$$

and

$$h = \cos^2\left(\frac{n\theta}{2}\right), \tag{14}$$

where n is a real number ≥ 0.

Figure 4 indicates geometric dependence of slip on n. The value $n=0$ corresponds to the NSBC for case A and a sphere with homogeneous slip length b for case B. When $n=1$, the slip length in both cases varies continuously from no slip at one pole to full slip at the other. This geometry closely approximates the ideal Janus sphere but differs significantly from the Janus configuration considered in the previous section because the slip length varies continuously across the surface. As n increases, the periodicity of slip and no-slip regions increases; the sphere becomes striped. This geometry approximates two distinct practical situations. First, engineered superhydrophobic surfaces often consist of periodic

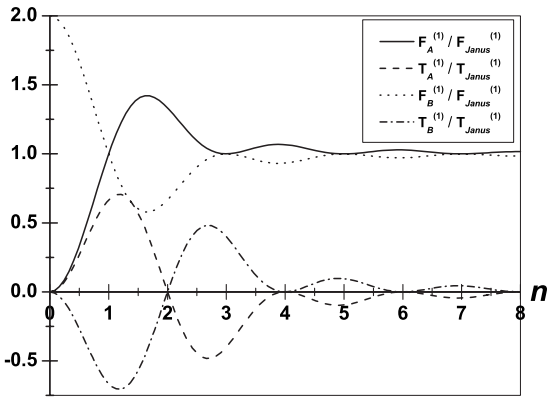

FIG. 5. Forces and torques on spheres with continuously varying surface patterning. Cases A and B refer to Eqs. (13) and (14), respectively, and the vertical axis is normalized relative to results for a discontinuous Janus particle [4].

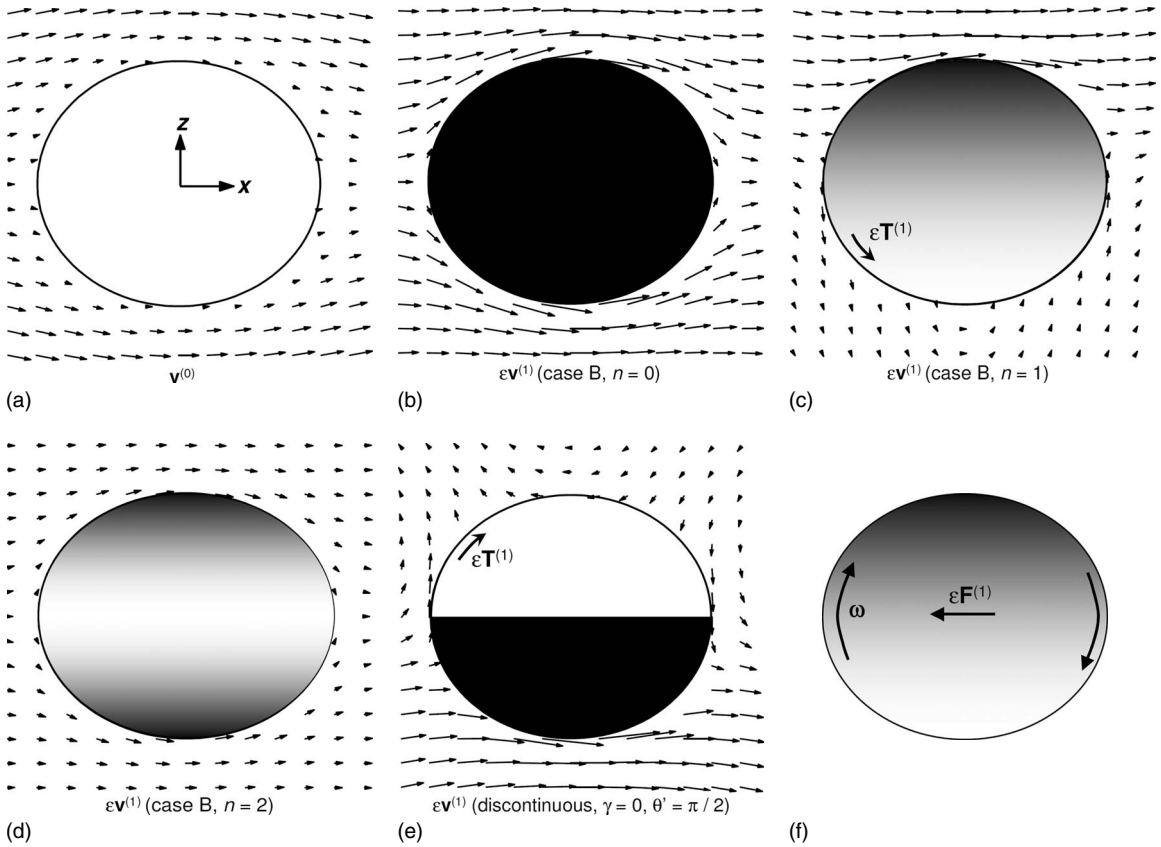

FIG. 6. Examples of predicted flow fields and dynamics in the plane $y=0$. The flow field for a sphere with the NSBC in unbounded uniform flow parallel to the positive x direction is plotted in (a). For a slip boundary condition, this flow field is modified by a first-order correction, which is plotted [(b)–(d)] for various instances of continuous slip boundary conditions and (e) for an ideal Janus particle. In figures (b) through (e), vectors are proportional to $\epsilon\mathbf{v}^{(1)}$, with consistent scaling of magnitude between figures. The arrows representing $\mathbf{v}^{(0)}$ in figure (a) have been shortened by a factor of b/a. (f) demonstrates the direction of the force on an asymmetric sphere (case B, $n=1$) rotating at angular velocity $\boldsymbol{\omega}$ in a quiescent fluid.

slip and no-slip ridges. Second, Janus-like [17,29] and ternary [33] particles can have well-defined and controlled periodicity.

Using the Legendre polynomial expansion as in the previous section, the first two spherical harmonics of g are

$$g(\theta) = g_0(\theta) + g_1(\theta) + \ldots = \frac{2n^2 - 1 + \cos(n\pi)}{4(n^2-1)} + \frac{3\cos\theta(\cos(n\pi)-1)}{4(n^2-4)} + \ldots . \quad (15)$$

In unbounded uniform flow of magnitude U_x parallel to the Cartesian x axis, the forces for cases A and B are, respectively,

$$\epsilon\mathbf{F}_A^{(1)} = \frac{b_\parallel}{a} 6\pi\eta a U_x \left(\frac{2n^2 - 1 + \cos(n\pi)}{4(n^2-1)}\right)\hat{\mathbf{x}}, \quad (16)$$

and

$$\epsilon\mathbf{F}_B^{(1)} = \frac{b_\parallel}{a} 6\pi\eta a U_x \left(\frac{2n^2 - 3 - \cos(n\pi)}{4(n^2-1)}\right)\hat{\mathbf{x}}. \quad (17)$$

The equivalent first-order torques are

$$\epsilon\mathbf{T}_A^{(1)} = \frac{b_\parallel}{a}\frac{9\pi\eta a^2 U_x}{2}\left(\frac{\cos(n\pi)-1}{n^2-4}\right)\hat{\mathbf{y}} = -\epsilon\mathbf{T}_B^{(1)}. \quad (18)$$

Equations (16)–(18) are plotted as a function of n in Fig. 5, with the vertical axis again normalized relative to the ideal discontinuous Janus sphere. The torque on a sphere is zero (due to symmetry) when n is an even number, and maximized when n is close to one. An extreme value in the lubrication force occurs near $n=1.5$ so there is an interesting region $0.5<n<1.5$ in which torque is nearly maximized and lubrication force varies widely, and could be tuned depending on the application considered. At large values of n, the force converges to the ideal Janus result, and the torque converges to zero because there is lack of asymmetry. As with the discontinuous boundary condition, the normalized force in purely rotational flow is equal to the normalized torque in unbounded uniform flow, and vice versa, for both cases A and B.

Figure 6 illustrates some important aspects of the predictions above. In the case of irrotational flow, there is a method for calculating $\mathbf{v}^{(1)}$ by explicitly deriving analytical spherical harmonics [1], allowing flow lines to be plotted. The velocity field is consistent with the calculated dynamics. Torque arises in irrotational flow only when there is asymmetry of

the boundary condition and flow field. Flow asymmetry is greater for the discontinuous boundary condition than the analogous continuous case, leading to greater torque. For the discontinuous asymmetric sphere [Fig. 6(e)], the first-order flow vector points in the negative x direction, opposing the incident flow, near the nonslip surface. The size of the $\epsilon \mathbf{v}^{(1)}$ vectors, and hence of the lubrication force, is much reduced for $n=2$ in comparison with $n=0$. Figure 6(f) demonstrates the direction of the force on a rotating asymmetric sphere. Due to linearity of the equations, superposition applies to the dynamics of a sphere in a flow with unbounded rotational and irrotational components.

V. DISCUSSION AND CONCLUSIONS

The calculated dynamic effects could be intentionally utilized in future applications of Janus spheres, and could have implications for currently envisaged applications. The torque, which allows manipulation of particle orientation in flow, is greatest when the boundary-condition asymmetry relative to the flow direction is maximized. Asymmetry is greater for a relatively sharp transition between slip and NSBC-surfaced hemispheres than for more continuous surface variation. In the range $0.5<n<1.5$, a particle experiences large torque and could have a lubrication force anywhere between 0.6 and 1.4 times the ideal Janus sphere value. In purely rotational flow, the role of asymmetry applies to force rather than torque so that a highly asymmetric particle can experience a linear impulse.

For superhydrophobic and inhomogeneous surfaces consisting of periodic stripes, there are important dynamic effects on the sphere when surface periodicity is of the same order of magnitude as the sphere ($n \lesssim 5$). Note that for small values of n, the superhydrophobic Cassie state could be distorted or difficult to achieve in practice due to curvature of the spherical surface. For higher pattern periodicity, the lubrication force is present but there is little torque on the sphere; at $n=5$, the local torque maximum is $\sim 10\%$ of the value for the ideal Janus sphere. We can therefore suggest a regime ($n \gtrsim 5$) in which striped patterning does not significantly affect the sphere dynamics. In this regime, the effective slip length of the surface should be considered, and the superhydrophobic patterning could itself be applied in geometrical surface patterns. There is the possibility that spheres patterned in stripes using Janus-like techniques [17,29] could give rise to a superhydrophobic surface, and therefore an effective slip length orders of magnitude higher than the intrinsic slip length. Note that the analysis accounts only for surface forces; nonspherical surface geometry due to ridges could cause other dynamic effects.

As with the general phenomenon of slip, the role of length scales is important in the present work. Although the limit $b \ll a$ was used in the present analysis, this is not a physical limitation. The prospect of a sphere patterned with a superhydrophobic surface of effective slip length greater than the sphere radius is interesting. The importance of Brownian motion, which limits slip-induced manipulation as explored in [4], is also dependent on length scale. Thermal effects do provide a physical limitation to the utility of engineered Janus particles. Enhanced effective slip lengths caused by high-periodicity patterning should be comparable to far-field slip lengths in analyses of superhydrophobic surfaces elsewhere [8,12–15]. It is possible that the dynamic effects could, to some extent, be effective at higher Reynolds number, and therefore macroscopic systems.

The present work predicts dynamic effects which are, as yet, untested in practice. It is hoped that the analysis will add to the design toolbox of the microfluidic or nanofluidic engineer. The manipulation method considered only requires application of directional (or rotational) flow but dynamic effects could also be considered in conjunction with manipulations using electric fields [24,35] and experimental techniques for investigating Janus sphere dynamics [22]. Future analytic or computational work could include azimuthal asymmetry, rotation, asphericity, and surface roughness [23], bounded or nonuniform flow, or the regime in which $b \sim a$. There is also potential for further exploration of analytic approaches to superhydrophobic surfaces.

[1] J. Happel and H. Brenner, *Low Reynolds Number Hydrodynamics* (Noordhoff International Publishing, The Netherlands, 1973).

[2] E. Lauga, M. P. Brenner, and H. A. Stone, *Handbook of Experimental Fluid Dynamics* (Springer, New York, 2005), Chap. 15.

[3] S. Senchenko and H. J. Keh, Phys. Fluids **18**, 088104 (2006).

[4] G. R. Willmott, Phys. Rev. E **77**, 055302(R) (2008).

[5] C. Neto, D. R. Evans, E. Bonaccurso, H.-J. Butt, and V. S. J. Craig, Rep. Prog. Phys. **68**, 2859 (2005).

[6] C. Cottin-Bizonne, A. Steinberger, B. Cross, O. Raccurt, and E. Charlaix, Langmuir **24**, 1165 (2008).

[7] C. I. Bouzigues, L. Bocquet, E. Charlaix, C. Cottin-Bizonne, B. Cross, L. Joly, A. Steinberger, C. Ybert, and P. Tabeling, Philos. Trans. R. Soc. London, Ser. A **366**, 1455 (2008).

[8] C. Ybert, C. Barentin, C. Cottin-Bizonne, P. Joseph, and L. Bocquet, Phys. Fluids **19**, 123601 (2007).

[9] C. Duez, C. Ybert, C. Barentin, C. Cottin-Bizonne, and L. Bocquet, J. Adhes. Sci. Technol. **22**, 335 (2008).

[10] D. Quéré and M. Reyssat, Philos. Trans. R. Soc. London, Ser. A **366**, 1539 (2008).

[11] R. S. Voronov, D. V. Papavassiliou, and L. L. Lee, Ind. Eng. Chem. Res. **47**, 2455 (2008).

[12] S. C. Hendy and N. J. Lund, Phys. Rev. E **76**, 066313 (2007).

[13] M. Sbragaglia and A. Prosperetti, Phys. Fluids **19**, 043603 (2007).

[14] C. J. Teo and B. C. Khoo, Microfluid. Nanofluid. (to be published).

[15] B. Woolford, D. Maynes, and B. W. Webb, Microfluid. Nanofluid. (to be published).

[16] E. Lauga and H. A. Stone, J. Fluid Mech. **489**, 55 (2003).

[17] S. C. Glotzer and M. J. Solomon, Nature Mater. **6**, 557 (2007).

[18] A. Perro, S. Reculusa, S. Ravaine, E. Bourgeat-Lami, and E. Duguet, J. Mater. Chem. **15**, 3745 (2005).
[19] A. Walther and A. H. E. Muller, Soft Matter **4**, 663 (2008).
[20] S. Pradhan, L. E. Brown, J. P. Konopelski, and S. Chen, J. Nanopart. Res. (2009).
[21] S. J. J. S. H. Kim, W. C. Jeong, H. S. Park, and S. M. Yang, Adv. Mater. **20**, 4129 (2008).
[22] S. M. Anthony, M. Kim, and S. Granick, Langmuir **24**, 6557 (2008).
[23] D. J. Adams, S. Adams, J. Melrose, and A. C. Weaver, Colloids Surf., A **317**, 360 (2008).
[24] S. Gangwal, O. J. Cayre, M. Z. Bazant, and O. D. Velev, Phys. Rev. Lett. **100**, 058302 (2008).
[25] S. Jiang, M. J. Schultz, Q. Chen, J. S. Moore, and S. Granick, Langmuir **24**, 10073 (2008).
[26] S. Jiang and S. Granick, Langmuir **24**, 2438 (2008).
[27] K.-H. Roh, M. Yoshida, and J. Lahann, Langmuir **23**, 5683 (2007).
[28] A. Walther, A. Göldel, and A. H. E. Müller, Polymer **49**, 3217 (2008).
[29] T. Higuchi, A. Tajima, K. Motoyoshi, H. Yabu, and M. Shimomura, Angew. Chem., Int. Ed. **47**, 8044 (2008).
[30] A. Perro, F. Meunier, V. Schmitt, and S. Ravainé, Colloids Surf., A **332**, 57 (2009).
[31] M. Lattuada and T. A. Hatton, J. Am. Chem. Soc. **129**, 12878 (2007).
[32] T. Isojima, M. Lattuada, J. B. V. Sande, and T. A. Hatton, ACS Nano **2**, 1799 (2008).
[33] Z. Nie, W. Li, M. Seo, S. Xu, and E. Kumacheva, J. Am. Chem. Soc. **128**, 9408 (2006).
[34] C. A. Serra and Z. Chang, Chem. Eng. Technol. **31**, 1099 (2008).
[35] D. Bratko, C. D. Daub, and A. Luzar, Faraday Discuss. **141**, 55 (2009).
[36] C. L. M. H. Navier, Mem. Acad. Sci. Inst. Fr. **6**, 839 (1827).
[37] D. Einzel, P. Panzer, and M. Liu, Phys. Rev. Lett. **64**, 2269 (1990).
[38] S. Jiang and S. Granick, J. Chem. Phys. **127**, 161102 (2007).